Nano Energy 77 (2020) 105158

Contents lists available at ScienceDirect

Nano Energy

journal homepage: http://www.elsevier.com/locate/nanoen

Isolated Ni single atoms in nitrogen doped ultrathin porous carbon templated from porous g-C_3N_4 for high-performance CO_2 reduction

Yan Lu [a,b], Haojing Wang [a], Pengfei Yu [c], Yifei Yuan [d], Reza Shahbazian-Yassar [d], Yuan Sheng [a,b], Shuyang Wu [a,b], Wenguang Tu [a], Guanyu Liu [a,b], Markus Kraft [b,e], Rong Xu [a,b,*]

[a] School of Chemical and Biomedical Engineering, Nanyang Technological University, 62 Nanyang Drive, Singapore, 637459, Singapore
[b] C4T CREATE, National Research Foundation, CREATE Tower, 1 Create Way, 138602, Singapore
[c] Shanghai Institute of Microsystem and Information Technology, Chinese Academy of Sciences, 865 Changning Road, Shanghai City, 200050, PR China
[d] Department of Mechanical and Industrial Engineering, University of Illinois at Chicago, Chicago, IL, 60607, United States
[e] Department of Chemical Engineering and Biotechnology, University of Cambridge, CB2 3RA, UK

ARTICLE INFO

Keywords:
Ni single atom
Nitrogen doped carbon
G-C_3N_4 template
Electrocatalyst
CO_2 electroreduction

ABSTRACT

Electrochemical reduction of CO_2 to value-added products is an effective approach to manage the global carbon balance. However, the lack of effective electrocatalyst for CO_2 reduction process is a major obstacle for its development. Currently, constructing atomically dispersed non-precious metal electrocatalysts presents a promising way to build high-performance and cost-effective electrochemical CO_2 reduction systems. Herein we demonstrate a novel strategy to realize the anchoring and stabilization of isolated Ni atoms in the nitrogen-doped ultrathin porous carbon nanosheets via a polydopamine-assisted g-C_3N_4 template method. Benefitting from the abundant atomic Ni sites and ultrahigh specific surface area of porous 2D supports (>1000 $m^2\ g^{-1}$), the catalyst exhibits excellent activity for CO_2 reduction with particularly high selectivity towards CO, achieving a faradaic efficiency of 96% at −0.86 V (vs. RHE) with a current density of 26.4 mA cm^{-2} in 0.1 M $KHCO_3$ solution.

Recently, electrochemically converting greenhouse CO_2 to value-added fuels and chemicals has attracted increasing attention in terms of its great significance for both environmental protection and energy crisis mitigation [1–3]. However, the extremely stable chemical bond in CO_2 (C═O, 806 kJ mol^{-1}) makes the electrochemical reduction of CO_2 highly challenging as it requires large overpotentials to overcome the activation barriers and under which, competitive side reactions such as the hydrogen evolution reaction (HER) can easily take place [4,5]. In this regard, finding robust catalysts with high activity, selectivity and stability is of paramount importance to realize the practical application of CO_2 electrochemical reduction [6].

Over the past decades, a large number of materials have been evaluated as catalysts for CO_2 electroreduction [7,8]. Among them, non-noble metal-based single-atom catalysts have shown great potential as promising high-efficiency and low-cost systems [9,10]. Thanks to the unique geometric and electronic properties stemming from the absence of metal-metal bonds and the cationic (or sometimes anionic) nature of the isolated catalytic sites, single-atom catalysts can exhibit much superior performance than their bulk counterparts in CO_2 reduction reaction (CO_2RR) [3,11–13]. However, the construction of single-atom catalysts remains a challenging task because of the high surface energy of single atoms.

Fabricating metal-nitrogen-carbon (M-N-C) moiety based materials with atomically dispersed M centres bonded to neighbouring N atoms in carbon-rich supports has been proved as an effective way to obtain single-atom catalysts, by which N atoms can anchor single M atoms and avoid their aggregation into nanoparticles during synthesis and reaction [4,14–18]. More importantly, the unique structure and coordination environment of the formed M-N-C moiety can endow them with favourable kinetics and excellent catalytic activities [5,14,19–22]. Up to date, some design strategies for such catalysts have been demonstrated, including ionic exchange of metal-organic-frameworks [15,23,24], topo-chemical transformation strategy [19], pyrolysis of metal complexes containing both N and C [12,25,26], and multistep pyrolysis method [27]. Despite these progresses, the synthesis of single atom catalysts is still in its infancy and strategies for control over the contents of singly active sites need to be improved. Further, unravelling the coordination environment and electronic structure of single-atom catalyst and understanding the structure-performance relationship at molecular level is particularly desirable, yet highly challenging.

* Corresponding author. School of Chemical and Biomedical Engineering, Nanyang Technological University, 62 Nanyang Drive, Singapore, 637459, Singapore.
E-mail address: rxu@ntu.edu.sg (R. Xu).

https://doi.org/10.1016/j.nanoen.2020.105158
Received 11 May 2020; Received in revised form 23 June 2020; Accepted 30 June 2020
Available online 25 July 2020

Herein, we demonstrate a novel strategy for the successful synthesis of a single-atom catalyst consisting of isolated Ni active centres anchoring on ultrathin porous N-doped carbon nanosheets (designated as NiSA/N–C) with excellent activity and selectivity for CO_2 reduction to CO. This synthesis relies on the use of polydopamine (PDA) as a unique anchoring agent, which is reported to have N-containing ligands for metal (such as Ni^{2+}, Cu^{2+}, Hg^{2+}, and so on) coordination [28–32], and can adhere to virtually all types of surfaces, regardless of the substrate chemistry [33–35]. Consequently, PDA can be easily coated on the surface of porous g-C_3N_4 template and subsequently anchor Ni^{2+} from the metal precursor solution under a mild condition [29]. The pre-formation of Ni^{2+}-PDA complex not only stabilizes the atomic metal centres during the subsequent pyrolysis, but also enables the formation of Ni–N coordination geometry by the N-containing moiety. Importantly, the content of Ni single atoms in the composite catalysts can be controlled by simply tuning the amount of Ni precursor. Furthermore, no additional acid-leaching process is required for removing metal nanoparticles which might compromise the property of the carbon support [4,14,20,36]. The atomically dispersed active sites, together with the large specific surface areas of the support boost the catalytic reaction, achieving a maximum conversion efficiency of 96% for CO with high current density and remarkable turnover frequency (TOF). Compared with previous reports using PDA to prepare single-atom catalysts [37,38], our method employs g-C_3N_4 as a self-sacrificial template, which adopts the advantages of both g-C_3N_4 and PDA, rendering the facile synthesis of single-atom catalysts with ultrahigh specific surface area. It is anticipated that this work may open new avenues for the design and synthesis of high efficiency electrocatalytic systems for CO_2 conversion reactions and hasten the practical implementation of CO_2 conversions.

A scheme illustrating the synthesis process of the catalyst is shown in Fig. 1. First, porous g-C_3N_4 nanosheets were prepared by thermal decomposition-polymerization of urea (Fig. S1). Then, the g-C_3N_4 template was dispersed in a tris-buffer solution and ultrasonicated for 30 min to form a light-yellow milky mixture. Subsequently, PDA was coated onto the surface of g-C_3N_4 template (PDA@g-C_3N_4) by adding dopamine precursor (dopamine hydrochloride, designated as DAH) in the mixture at room temperature. During this process, an apparent colour change from light yellow to dark grey was observed, indicating the successful adhesion of PDA layer onto g-C_3N_4 template. After that, PDA@g-C_3N_4 was collected and re-dispersed into Ni^{2+} containing aqueous solution with a precursor weight ratio of 7.24 wt% (Ni^{2+}/DAH) (Table S1). By virtue of the chelating property of PDA, Ni^{2+} is easily anchored and forms Ni^{2+}-PDA@g-C_3N_4 precursor. Finally, Ni single atoms anchored on nitrogen doped ultrathin porous carbon nanosheets (NiSA/N–C) were obtained by pyrolysis of Ni^{2+}-PDA@g-C_3N_4 precursor at 1000 °C in N_2 atmosphere. During which, PDA coating was carbonized and g-C_3N_4 template was decomposed and converted to nitrogen doped carbon skeleton [39]. Most importantly, the isolated Ni^{2+} ions were stabilized by N coordination and further reduced by the surrounding carbon, forming atomically dispersed active centres.

The as-prepared NiSA/N–C possesses an ultrathin porous two dimensional (2D) structure with wrinkled surfaces as revealed by field emission scanning electron microscopy (FESEM) and transmission electron microscopy (TEM) images (Fig. 2a and b), which is nearly the same as that observed for the nitrogen doped ultrathin porous carbon nanosheets (N–C) support without loading of Ni species (Fig. S2). Disordered graphene lattices are observed in the HRTEM image with lattice spacing measured to be around 0.34 nm (Fig. 2c), indicating the partial graphitization of N–C support (also evidenced by Raman spectrum in Fig. S3). The corresponding selected area electron diffraction (SAED, inset of Fig. 2c) pattern displays diffraction rings that are consistent with the typical hexagonal pattern of graphene with poor crystallinity [40,41]. Notably, Ni nanoparticles are not observed under both FESEM and TEM observations, implying that Ni species are highly dispersed at sub-nanometer scale on the carbon nanosheets. This is confirmed by aberration-corrected high-angle annular dark field scanning transmission electron microscopy (HAADF-STEM) images, in which bright spots corresponding to single Ni atoms are well observed across the entire carbon nanosheets, demonstrating the atomic dispersion of Ni in NiSA/N–C (Fig. 2d and e). Element mapping images indicate the homogeneous distribution of Ni and N species in carbon nanosheets (Fig. 2f), confirming the formation of nitrogen doped carbon nanosheets. N doping here is considered to play a critical role in trapping and bonding a significant number of Ni atoms in the N–C support. The actual loading of Ni is 0.86 wt% as determined by ICP-AES. The specific surface area of NiSA/N–C is 1009.2 $m^2\ g^{-1}$, which is much higher than that of the g-C_3N_4 template (63.5 $m^2\ g^{-1}$) and comparable to that of N–C itself (1081.1 $m^2\ g^{-1}$) (Figs. S4a and b and Table S2). One can see that there are no characteristic peaks of Ni crystals in the XRD pattern of NiSA/N–C (Fig. S5), further confirming the absence of Ni nanoparticles in NiSA/N–C. The presence of a broad peak at around 25–26° indicates the formation of graphitic carbon, which is consistent with the observation of the lattice fringes in Fig. 2c. Notably, our strategy offers the unique advantage in controlling the loading of single-atom species by simply tuning the amount of precursor during the synthesis. For instance, samples with atomic Ni loadings of 0.50 wt% (0.05xNiSA/N–C) and 4.26 wt% (10xNiSA/N–C) (Figs. S5c–d, Figs. S6–S7 and Table S2) have been successfully synthesized at precursor weight ratios of 0.362 wt% and 72.4 wt% (Table S1), respectively.

To identify the critical role of PDA in achieving single atom dispersion, two control experiments were carried out. In the first experiment, Ni^{2+} precursor and DAH were added simultaneously at the ratio of 7.24 wt% (same with that for NiSA/N–C) in the reaction system. In this case, polymerization of dopamine was promoted because of the catalytic effect of Ni^{2+} [32], which resulted in an uncontrollable anchoring of Ni^{2+} and formation of Ni nanoparticles in the subsequent pyrolysis process (NiNP/N–C, Fig. S5e and Figs. S8a–c). In the second control experiment, a physical mixture of $Ni(NO_3)_2{\cdot}6H_2O$ and PDA@g-C_3N_4 (same precursor weight ratio) was pyrolyzed. Ni nanoparticles dispersed on nitrogen

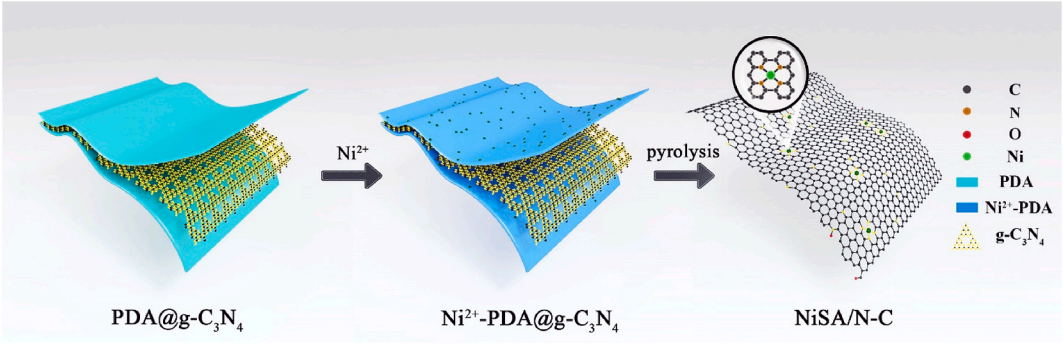

Fig. 1. Schematic illustration of the synthesis of NiSA/N–C.

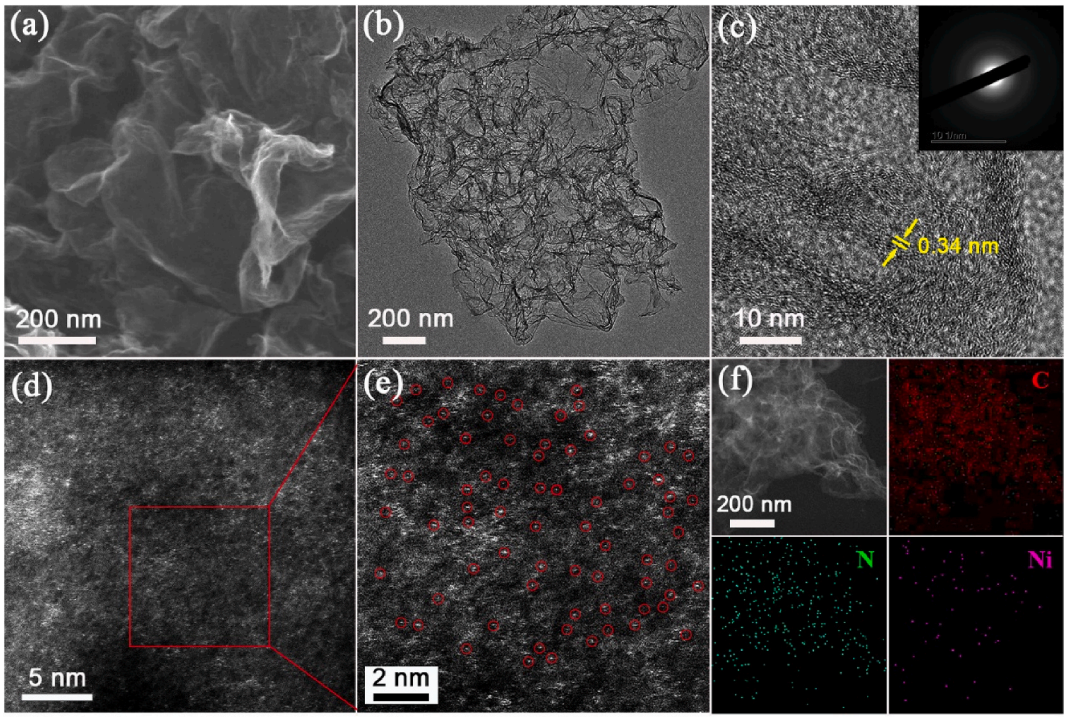

Fig. 2. (a) FESEM, (b) TEM, and (c) HRTEM images of NiSA/N–C with 0.86 wt% Ni loading (inset of c is the corresponding SAED pattern). (d,e) Magnified HAADF-STEM images of NiSA/N–C. Ni single-atoms are marked with red circles. (f) EDS maps revealing the homogeneous distribution of Ni and N on the carbon support. (For interpretation of the references to colour in this figure legend, the reader is referred to the Web version of this article.)

doped carbon consisting of carbon nanosheets and carbon nanotubes (NiNP/N-CM, Fig. S5f and Figs. S8d–f) were obtained given poor interaction between Ni^{2+} and PDA at the solid state. Given the above results, it is speculated that PDA can anchor suitable amount of Ni^{2+} species from the precursor solutions [42] and guarantee the formation of atomically dispersed Ni species even after the high temperature pyrolysis process [30].

The bonding states of Ni, N and C in NiSA/N–C are investigated by soft X-ray absorption spectroscopy (sXAS) and X-ray photoelectron spectroscopy (XPS). As revealed in Fig. S9a, NiSA/N–C possesses a very similar Ni L_3 and L_2 edge sXAS profile to that of Ni Phthalocyanine (NiPc). Specifically, the main peak A at Ni L_3 edge is very sharp, indicating the lowest 3d unoccupied state is very local. The asymmetric feature of peak A in region A_1 implies the formation of π bond between Ni 3d and N 2p orbitals, which is often accompanied by a charge transfer from the metal atom into the ligand [43–45]. In addition, the small peaks observed in the range from 858 to 865 eV might be attributed to the bonding interaction between Ni 4sp and N 2p orbitals. The interaction between Ni and N can also be confirmed by the N 1s XPS in Fig. S10a. The N1s spectra could be deconvolved into three peaks, corresponding to pyridinic-N, graphitic-N, and pyridinic N^+-O^-, respectively. The absence of pyrrolic N might be ascribed to the carbonization at a high temperature of 1000 °C, which agrees with previous reports [39,46–48]. Compared with N–C, the peak assigned to pyridinic-N in single-atom catalysts shifts to the higher energy side, implying Ni bonding with pyridinic N (Fig. S10a) [19]. Such an interaction between Ni and N is further clarified by the observation of an additional feature (N_1 peak in Fig. S9b) in N *K*-edge profile of NiSA/N–C when comparing with that of N–C. This feature is corresponding to the observed character in region A1 at Ni L_3 edge, further evidencing the formation of π bond between Ni and neighbouring N in NiSA/N–C. In addition, C K-edge profiles and C1s XPS are also investigated. By comparison, C1s sXAS of NiSA/N–C is almost the same with that of N–C (Fig. S9c), excluding the formation of Ni–C bond, which can be also supported by the C1s XPS results (Fig. S10b).

To determine the detailed electronic structure and coordination environment around Ni sites, Synchrotron-based X-ray absorption near-edge structure (XANES) and extended X-ray absorption fine structure (EXAFS) of NiSA/N–C were examined. The absorption edge position of NiSA/N–C is located between that of Ni foil and NiO as indicated by red arrow in Fig. 3a, suggesting the valence of Ni species is situated between Ni(0) and Ni(II) [49,50]. The Ni K-edge exhibits a similar near edge structure to that of nickel phthalocyanine (NiPc), indicating that the coordination atoms for Ni sites should be those with a weaker electronegativity than O, such as C and N. As can be seen in the Fourier transform (FT) k3-weighted χ(k) function of the EXAFS spectra (Fig. 3b), NiSA/N–C only exhibits one dominant peak at 1.44 Å, ascribed to Ni–N coordination, proving the atomic dispersion of single Ni sites. In contrast, NiNP/N–C shows a main peak around 2.11 Å, which belongs to the Ni–Ni coordination. Further, the absence of a peak around 2.5 Å compared with that observed in NiPc precludes the formation of Ni–C coordination, which is consistent with the results analysed from C1s sXAS (Fig. S9c) and C1s XPS (Fig. S10b). The wavelet transform (WT) plot of NiSA/N–C shows the WT maximum at 5.5 $Å^{-1}$, which is corresponding to the Ni–N bonding by comparing with that for Ni foil, NiO, NiNP/N–C and NiPc (Fig. 3c). There is no intensity maximum corresponding to Ni–Ni bonding observed for NiSA/N–C, further confirming its single-atom feature. The coordination configuration of Ni atom is speculated to be Ni–N_4 according to the EXAFS fitting results (Fig. 3d, Table S3), which is consistent with previous reports on Ni–N active centres [4,19,27,37]. Combining with the previous verification that there are no Ni–C bonds in NiSA/N–C (Figs. S9–10), the structural model of our Ni catalyst is proposed as shown in Fig. 3d.

We next evaluate the CO_2RR activities of the as-prepared catalysts in a H-type electrochemical cell separated by a Nafion 117 membrane. As can be seen from the linear sweep voltammetry (LSV) curves, NiSA/N–C with Ni–N_4 active sites exhibits extremely high electrocatalytic activity for CO_2RR, evidenced by a large current density of 80.2 mA cm^{-2} at −1.0 V, which is more than 2 times of those for Ni NPs catalysts (Fig. S11a) and 4.5 times of that for the pristine N–C (Fig. 4a). This value

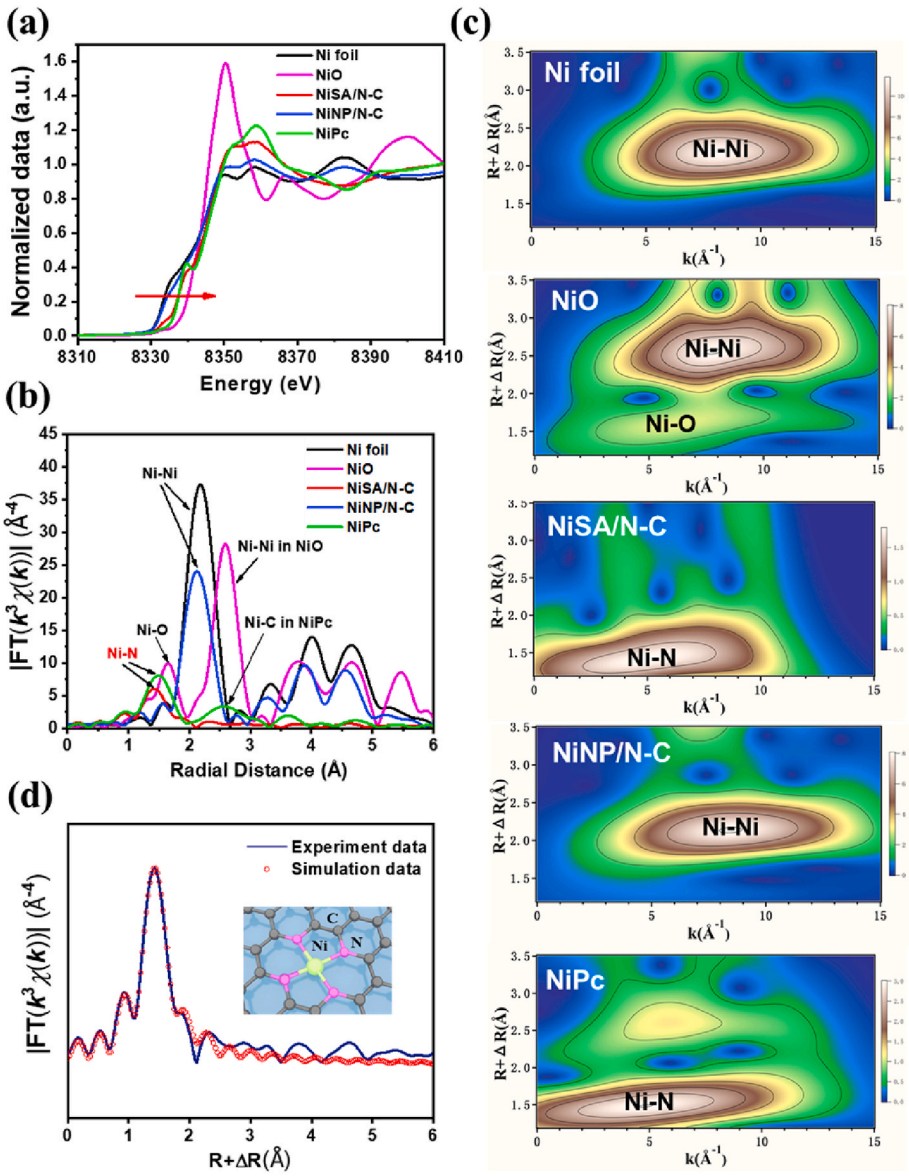

Fig. 3. (a) XANES spectra and (b) Fourier transform (FT) at the Ni K-edge of Ni foil, NiO, NiSA/N–C, NiNP/N–C and NiPc. (c) Wavelet transform (WT) of Ni foil, NiO, NiSA/N–C, NiNP/N–C and NiPc. (d) The corresponding EXAFS R space fitting curves of NiSA/N–C (inset shows the structure of the nickel site in NiSA/N–C; the balls in green, pink and grey represent Ni, N and C atoms, respectively). (For interpretation of the references to colour in this figure legend, the reader is referred to the Web version of this article.)

is also larger than most of the previously reported CO_2 electroreduction catalysts (Table S4). When tested in a concentrated electrolyte with 0.5 M $KHCO_3$, an even higher current density of 111.5 mA cm^{-2} is reached at −1.0 V for NiSA/N–C (Fig. S12a). It is noteworthy that the electrochemical activity of Ni single-atom catalysts is not simply related to the contents of Ni species as suggested by the results that NiSA/N–C shows larger current density than those of other single Ni atom catalysts (26 mA cm^{-2} at −1.0 V for 0.05xNiSA/N–C and 50 mA cm^{-2} at −1.0 V for 10xNiSA/N–C). It is understandable that NiSA/N–C with more active centres shows better performance than 0.05xNiSA/N–C. While for the one with a high Ni loading of 4.26 wt%, the inferior performance might be due to the reduction of mono-dispersibility of Ni species, which can be evidenced by the observation of aggregates consisted of several atoms under magnified HAADF-STEM image (Fig. S7e). Another possible reason might be ascribed to the less percentage of N in 10xNiSA/N–C than that in NiSA/N–C (Table S2), which would lead to a lower conductivity of the N–C support [51,52]. This can be also evidenced by the electrochemical impedance spectroscopy (EIS) measurements (Fig. S13) that a larger internal resistance is observed in 10xNiSA/N–C than that in NiSA/N–C. In this consideration, controlled synthesis of single-atom catalysts with optimized metal contents is crucial for obtaining high-performance CO_2 reduction catalysts, which indicates the advantage of our synthesis strategy.

The measurement of faradaic efficiency (FE) was further carried out to evaluate the selectivity of the prepared catalysts for CO_2 reduction. Gas chromatography analyses suggested that the primary reduction products for all catalysts are CO and H_2. Trace of CH_4 was also detected during the CO_2 reduction, which leads to the sum FE of CO and H_2 less than 100% (Fig. 4b and Fig. S14). There was no liquid product detected by ^1H nuclear magnetic resonance spectroscopy (Fig. S15). Particularly, in the case of metallic nickel catalyst, it has been reported to have a trend to produce H_2 because of its strong *H binding [18,53,54]. This is consistent with the case of NiNP/N–C and NiNP/N-CM, which only show maximum faradaic efficiency (FE) for CO (FE_{CO}) of 86% (−0.86 V) and 84% (−0.86 V) (Fig. S11b), respectively. In strong contrast, when Ni species are engineered to be in atomically dispersed Ni–N_4 centres, a FE_{CO} of 96% is obtained for NiSA/N–C at −0.86 V (Fig. 4b), which is much higher than that of metallic Ni catalysts (NiNP/N–C and NiNP/N-CM), showing the excellent selectivity of Ni–N_4 centres. This might be attributed to the low binding energy toward *H and low-to-no binding of *CO, according to DFT simulations [18,55,56]. Notably, NiSA/N–C also exhibits remarkable performance in 0.5 M $KHCO_3$ with

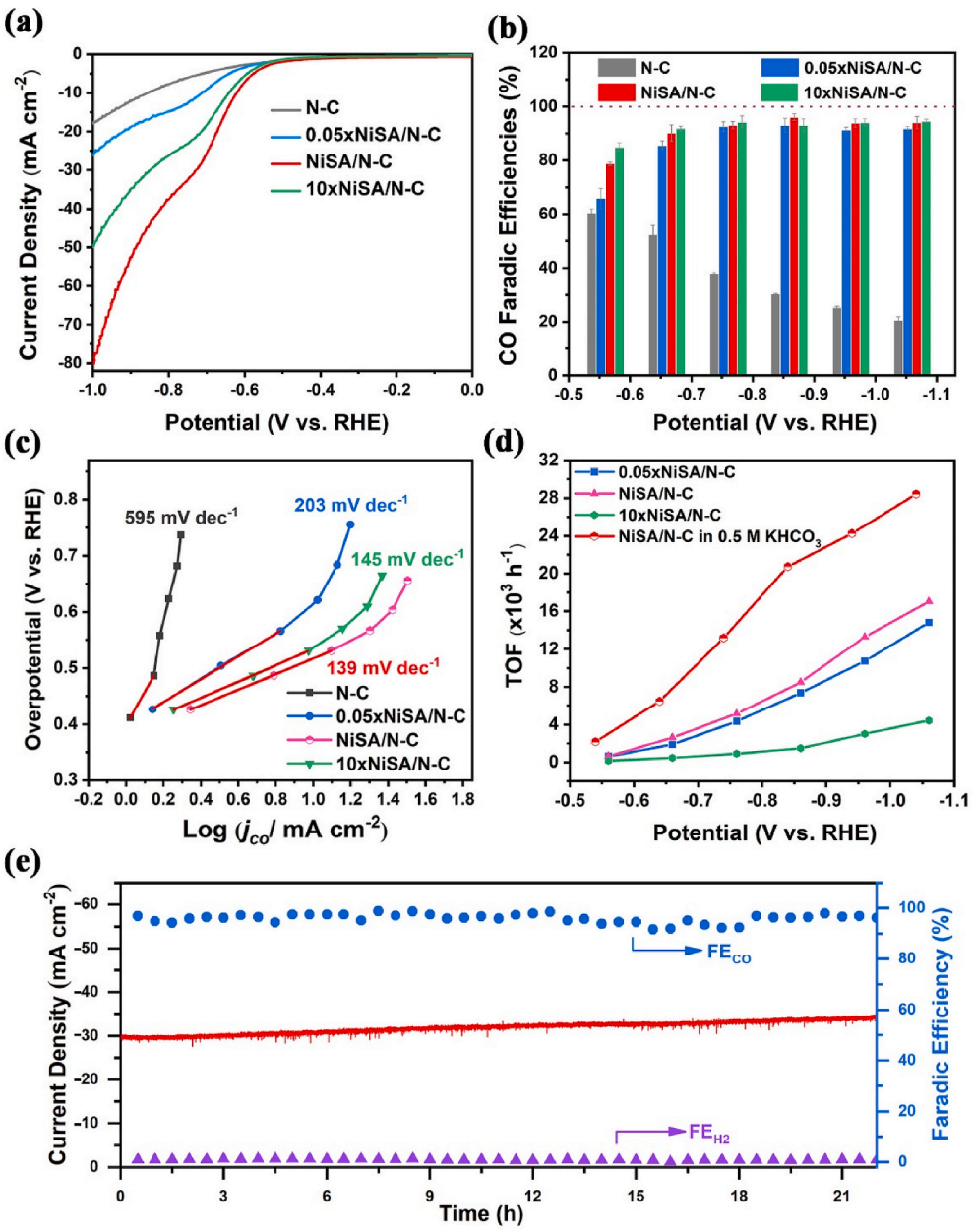

Fig. 4. (a) LSV curves at a scan rate of 10 mV s^{-1}, (b) FEs of CO and (c) Tafel plots for N–C, 0.05xNiSA/N–C, NiSA/N–C, and 10xNiSA/N–C catalysts tested in CO_2-saturated 0.1 M $KHCO_3$ electrolytes. (d) TOFs of 0.05xNiSA/N–C, NiSA/N–C, and 10xNiSA/N–C samples in CO_2-saturated 0.1 M $KHCO_3$ electrolytes and NiSA/N–C sample in CO_2-saturated 0.5 M $KHCO_3$ electrolyte at different applied potentials. (e) Stability of NiSA/N–C at a potential of −0.86 V vs. RHE during 22 h in CO_2-saturated 0.1 M $KHCO_3$ electrolyte.

the highest FE_{CO} of 94% achieved at −0.84 V (Fig. S12b), which is higher than many reported atomic Ni-based catalysts as compared in Table S4. Besides, comparable selectivity with similar FE_{CO} values has been obtained for the as-prepared three single-atom catalysts (Fig. 4b). On the contrary, the pristine N–C matrix shows very poor selectivity towards CO, demonstrating that the electrocatalytic activity for CO_2 reduction comes from Ni–N sites (Fig. 4b). This is further proved by the poison experiment for NiSA/N–C, where SCN^- was adopted as poison ion to metal sites (Fig. S16). The remarkable depression of catalytic activity for NiSA/N–C by adding SCN^- could be attributed to blocking of Ni atoms by SCN^-, thus confirming the active site role of the $Ni–N_4$ structure. In addition, the suppressed H_2 evolution over NiSA/N–C compared with other catalysts can be clearly observed (Fig. S11b and Fig. S14).

To get insight into the reaction mechanism of NiSA/N–C, Tafel slope was examined. For NiSA/N–C, a Tafel slope of 139 mV dec^{-1} was obtained, suggesting that the initial one-electron reduction of CO_2, which generates the $CO_2^{\bullet-}$ key intermediate, is the rate-determining step for CO evolution [1,57–59]. Besides, a smaller Tafel slope indicates the better catalytic performance. Accordingly, NiSA/N–C shows the smallest Tafel slope compared with other catalysts (145, 203 and 595 mV dec^{-1} for 0.05xNiSA/N–C, 10xNiSA/N–C and N–C, respectively) (Fig. 4c), indicating its most favourable kinetics for CO_2 reduction. In addition, the Nyquist plots in Fig. S13 also demonstrate that NiSA/N–C has the smallest resistance, which would lead to remarkably enhanced activity for CO_2 reduction.

NiSA/N–C gives the highest TOF values over all potentials among the prepared catalysts (Fig. 4d and Fig. S11c). Specifically, TOF values of 8483 h^{-1} and 20752 h^{-1} are achieved when tested in 0.1 M $KHCO_3$ at −0.86 V and 0.5 M $KHCO_3$ at −0.84 V, respectively, which are also much higher than most of the reported catalysts (Table S4). Although several reported atomic Ni catalysts (Ref. S11, S12, S14 in Table S4) show higher TOF values than our NiSA@N–C sample, their other properties are inferior. Those performance comparisons further highlight the excellent catalytic performance of the $Ni–N_4$ structure. During the stability test, no obvious decay in FE_{CO} and current density was detected for

NiSA/N–C at a set potential of −0.86 V (Fig. 4e), indicating the excellent chemical stability of the Ni sites in NiSA/N–C for potential practical use. The slight increase of current density is most probably due to the increase of electrolyte temperature during the course of stability test. The good stability is also evidenced by the comparison of Ni 2p spectra for NiSA/N–C before and after test, which shows no obvious peak shifts (Fig. S17a). Further, the structure and morphology of the post-electrolysis of NiSA/N–C were also well maintained even after a long-term test as revealed by FESEM and TEM observations (Figs. S17b–e), demonstrating again the robust of the prepared catalyst.

In summary, we have developed a PDA-assisted method for facile preparation of supported metal catalysts with atomic dispersion, controllable loading, and ultra-high surface areas. Ni SAs are stabilized by the N-doped porous carbon support derived from pyrolysis of PDA coated g-C_3N_4 template. Significantly, NiSA/N–C with Ni–N_4 active centres demonstrates excellent activity in the conversion of CO_2 to CO with remarkably high selectivity, current densities and TOF values. We anticipate that our work may open a new avenue for the design and synthesis of supported SA metal catalysts with controllable metal loadings for a variety of applications.

Declaration of competing interest

The authors declare that they have no known competing financial interests or personal relationships that could have appeared to influence the work reported in this paper.

CRediT authorship contribution statement

Yan Lu: Conceptualization, Methodology, Formal analysis, Software, Data curation, Investigation, Visualization, Writing - original draft, Writing - review & editing. **Haojing Wang:** Investigation, Formal analysis, Software, Data curation. **Pengfei Yu:** Methodology, Formal analysis, Software, Data curation. **Yifei Yuan:** Methodology, Formal analysis, Software. **Reza Shahbazian-Yassar:** Writing - review & editing, Funding acquisition. **Yuan Sheng:** Methodology, Formal analysis. **Shuyang Wu:** Formal analysis, Data curation. **Wenguang Tu:** Formal analysis, Software. **Guanyu Liu:** Software, Data curation. **Markus Kraft:** Supervision, Funding acquisition. **Rong Xu:** Conceptualization, Methodology, Project administration, Supervision, Funding acquisition, Writing - review & editing.

Acknowledgements

The authors acknowledge the financial support from Singapore National Research Foundation (NRF) through the Cambridge Centre for Carbon Reduction in Chemical Technology (C4T) CREATE Program. R. Shahbazian-Yassar and Y. Yuan acknowledge the financial support from National Science Foundation (NSF) DMR-1809439. This work made use of instruments in the Electron Microscopy Service (Research Resources Centre, UIC). The authors would like to thank Prof. X. S. Zheng for the help on the fitting of XAS results.

Appendix A. Supplementary data

Supplementary data to this article can be found online at https://doi.org/10.1016/j.nanoen.2020.105158.

References

[1] D.D. Zhu, J.L. Liu, S.Z. Qiao, Adv. Mater. 28 (2016) 3423–3452.
[2] J.L. Qiao, Y.Y. Liu, F. Hong, J.J. Zhang, Chem. Soc. Rev. 43 (2014) 631–675.
[3] A.Q. Wang, J. Li, T. Zhang, Nat. Rev. Chem. 2 (2018) 1.
[4] H.B. Yang, S.F. Hung, S. Liu, K.D. Yuan, S. Miao, L.P. Zhang, X. Huang, H.Y. Wang, W.Z. Cai, R. Chen, J. Gao, X. Yang, W. Chen, Y. Huang, H.M. Chen, C.M. Li, T. Zhang, B. Liu, Nat. Energy 3 (2018) 140.
[5] K. Jiang, S. Siahrostami, T.T. Zheng, Y.T. Hu, S. Hwang, E. Stavitski, Y. Peng, J. Dynes, M. Gangisetty, D. Su, K. Attenkofer, H.T. Wang, Energy Environ. Sci. 11 (2018) 893–903.
[6] Z.W. Seh, J. Kibsgaard, C.F. Dickens, I. Chorkendorff, J.K. Nørskov, T.F. Jaramillo, Science 355 (2017), eaad4998.
[7] H. Mistry, A.S. Varela, S. Kuehl, P. Strasser, B.R. Cuenya, Nat. Rev. Mater. 1 (2016) 16009.
[8] L. Zhang, Z.J. Zhao, J.L. Gong, Angew. Chem. Int. Ed. 56 (2017) 11326–11353.
[9] S. Dou, X. Wang, S.Y. Wang, Small Methods 3 (2019) 1800211.
[10] K. Mou, Z. Chen, X. Zhang, M. Jiao, X. Zhang, X. Ge, W. Zhang, L. Liu, Small (2019) 1903668.
[11] Y.J. Chen, S.F. Ji, C. Chen, Q. Peng, D.S. Wang, Y.D. Li, Joule 2 (2018) 1242–1264.
[12] H. Yang, L. Shang, Q. Zhang, R. Shi, G.I. Waterhouse, L. Gu, T. Zhang, Nat. Commun. 10 (2019) 1–9.
[13] C. Zhang, S. Yang, J. Wu, M. Liu, S. Yazdi, M. Ren, J. Sha, J. Zhong, K. Nie, A. S. Jalilov, Z. Li, H. Li, B.I. Yakobson, Q. Wu, E. Ringe, H. Xu, P.M. Ajayan, J. M. Tour, Adv. Energy Mater. 8 (2018) 1703487.
[14] X.N. Li, X. Huang, S.B. Xi, S. Miao, J. Ding, W.Z. Cai, S. Liu, X.L. Yang, H.B. Yang, J. J. Gao, J. Wang, Y. Huang, T. Zhang, B. Liu, J. Am. Chem. Soc. 140 (2018) 12469–12475.
[15] C.M. Zhao, X.Y. Dai, T. Yao, W.X. Chen, X.Q. Wang, J. Wang, J. Yang, S.Q. Wei, Y. Wu, Y.D. Li, J. Am. Chem. Soc. 139 (2017) 8078–8081.
[16] H. Fei, J. Dong, D. Chen, T. Hu, X. Duan, I. Shakir, Y. Huang, X. Duan, Chem. Soc. Rev. 48 (2019) 5207–5241.
[17] W. Liu, Y. Chen, H. Qi, L. Zhang, W. Yan, X. Liu, X. Yang, S. Miao, W. Wang, C. Liu, A. Wang, J. Li, T. Zhang, Angew. Chem. Int. Ed. 57 (2018) 7071–7075.
[18] A.S. Varela, W. Ju, A. Bagger, P. Franco, J. Rossmeisl, P. Strasser, ACS Catal. 9 (2019) 7270–7284.
[19] X.G. Li, W.T. Bi, M.L. Chen, Y.X. Sun, H.X. Ju, W.S. Yan, J.F. Zhu, X.J. Wu, W. S. Chu, C.Z. Wu, Y. Xie, J. Am. Chem. Soc. 139 (2017) 14889–14892.
[20] K. Jiang, S. Siahrostami, A.J. Akey, Y.B. Li, Z.Y. Lu, J. Lattimer, Y.F. Hu, C. Stokes, M. Gangishetty, G.X. Chen, Y. Zhou, W. Hill, W.-B. Cai, D. Bell, K. Chan, J. K. Nørskov, Y. Cui, H. Wang, Inside Chem. 3 (2017) 950–960.
[21] Y. Sun, L. Silvioli, N.R. Sahraie, W. Ju, J. Li, A. Zitolo, S. Li, A. Bagger, L. Arnarson, X. Wang, T. Moeller, D. Bernsmeier, J. Rossmeisl, F.d.r. Jaouen, P. Strasser, J. Am. Chem. Soc. 141 (2019) 12372–12381.
[22] T. Möller, W. Ju, A. Bagger, X. Wang, F. Luo, T.N. Thanh, A.S. Varela, J. Rossmeisl, P. Strasser, Energy Environ. Sci. 12 (2019) 640–647.
[23] Z.B. Liang, C. Qu, D.G. Xia, R.Q. Zou, Q. Xu, Angew. Chem. Int. Ed. 57 (2018) 9604–9633.
[24] W. Ren, X. Tan, W. Yang, C. Jia, S. Xu, K. Wang, S.C. Smith, C. Zhao, Angew. Chem. Int. Ed. 58 (2019) 6972–6976.
[25] Y. Pan, R. Lin, Y.J. Chen, S.J. Liu, W. Zhu, X. Cao, W.X. Chen, K.L. Wu, W. C. Cheong, Y. Wang, L. Zheng, J. Luo, Y. Lin, Y. Liu, C. Liu, J. Li, Q. Lu, X. Chen, D. Wang, Q. Peng, C. Chen, Y. Li, J. Am. Chem. Soc. 140 (2018) 4218–4221.
[26] X. Rong, H.-J. Wang, X.-L. Lu, R. Si, T.-B. Lu, Angew. Chem. Int. Ed. 59 (2020) 1961–1965.
[27] Y. Cheng, S.Y. Zhao, B. Johannessen, J.P. Veder, M. Saunders, M.R. Rowles, M. Cheng, C. Liu, M.F. Chisholm, R. De Marco, H.M. Cheng, S. Yang, S.P. Jiang, Adv. Mater. 30 (2018) 1706287.
[28] S. Zhang, Y. Zhang, G. Bi, J. Liu, Z. Wang, Q. Xu, H. Xu, X. Li, J. Hazard Mater. 270 (2014) 27–34.
[29] J. Gao, H. Lei, Z. Han, Q. Shi, Y. Chen, Y. Jiang, Sci. Rep. 7 (2017) 45215.
[30] X. Fang, J. Li, X. Li, S. Pan, X. Zhang, X. Sun, J. Shen, W. Han, L. Wang, Chem. Eng. J. 314 (2017) 38–49.
[31] J. Kong, S.I.S. Shahabadi, X. Lu, Nanoscale 8 (2016) 1770–1788.
[32] L. Yang, J. Kong, D. Zhou, J.M. Ang, S.L. Phua, W.A. Yee, H. Liu, Y. Huang, X. Lu, Chem. Eur J. 20 (2014) 7776–7783.
[33] H. Lee, S.M. Dellatore, W.M. Miller, P.B. Messersmith, Science 318 (2007) 426–430.
[34] Y.L. Liu, K.L. Ai, L.H. Lu, Chem. Rev. 114 (2014) 5057–5115.
[35] Q. Ye, F. Zhou, W.M. Liu, Chem. Soc. Rev. 40 (2011) 4244–4258.
[36] F. Li, G.F. Han, H.J. Noh, S.J. Kim, Y.L. Lu, H.Y. Jeong, Z.P. Fu, J.B. Baek, Energy Environ. Sci. 11 (2018) 2263.
[37] M. Zhang, Y.-G. Wang, W. Chen, J. Dong, L. Zheng, J. Luo, J. Wan, S. Tian, W.-C. Cheong, D. Wang, J. Am. Chem. Soc. 139 (2017) 10976–10979.
[38] A. Han, W. Chen, S. Zhang, M. Zhang, Y. Han, J. Zhang, S. Ji, L. Zheng, Y. Wang, L. Gu, Adv. Mater. 30 (2018) 1706508.
[39] H.J. Yu, L. Shang, T. Bian, R. Shi, G.I. Waterhouse, Y.F. Zhao, C. Zhou, L.Z. Wu, C. H. Tung, T.R. Zhang, Adv. Mater. 28 (2016) 5080–5086.
[40] J. Jin, F. Pan, L. Jiang, X. Fu, A. Liang, Z. Wei, J. Zhang, G. Sun, ACS Nano 8 (2014) 3313–3321.
[41] R. Paul, Q. Dai, C. Hu, L. Dai, Carbon Energy 1 (2019) 19–31.
[42] J. Yang, K. Ni, D. Wei, Y. Ren, Biotechnol. Bioproc. Eng. 20 (2015) 901–907.
[43] S. Krasnikov, A. Preobrajenski, N. Sergeeva, M. Brzhezinskaya, M. Nesterov, A. Cafolla, M. Senge, A. Vinogradov, Chem. Phys. 332 (2007) 318–324.
[44] T. Hatsui, Y. Takata, N. Kosugi, J. Synchrotron Radiat. 6 (1999) 376–378.
[45] P.S. Johnson, J.M. García-Lastra, C.K. Kennedy, N.J. Jersett, I. Boukahil, F. Himpsel, P.L. Cook, J. Chem. Phys. 140 (2014) 114706.
[46] L.F. Chen, X.D. Zhang, H.W. Liang, M.G. Kong, Q.F. Guan, P. Chen, Z.Y. Wu, S. H. Yu, ACS Nano 6 (2012) 7092–7102.
[47] Y. Xu, C.L. Zhang, M. Zhou, Q. Fu, C.X. Zhao, M.H. Wu, Y. Lei, Nat. Commun. 9 (2018), https://doi.org/10.1038/s41467-41018-04190-z.
[48] F.B. Su, C.K. Poh, J.S. Chen, G.W. Xu, D. Wang, Q. Li, J.Y. Lin, X.W. Lou, Energy Environ. Sci. 4 (2011) 717–724.

[49] H.J. Qiu, Y. Ito, W. Cong, Y. Tan, P. Liu, A. Hirata, T. Fujita, Z. Tang, M. Chen, Angew. Chem. Int. Ed. 54 (2015) 14031–14035.
[50] L.L. Fan, P.F. Liu, X.C. Yan, L. Gu, Z.Z. Yang, H.G. Yang, S.L. Qiu, X.D. Yao, Nat. Commun. 7 (2016) 10667.
[51] Z.S. Wu, W. Ren, L. Xu, F. Li, H.-M. Cheng, ACS Nano 5 (2011) 5463–5471.
[52] L. Lin, J. Li, Q. Yuan, Q. Li, J. Zhang, L. Sun, D. Rui, Z. Chen, K. Jia, M. Wang, Yanfeng Zhang, Mark H. Rummeli, Ning Kang, H.Q. Xu, Feng Ding, Hailin Peng, Z. Liu, Sci. Adv. 5 (2019) eaaw8337.
[53] L. Gong, D. Zhang, C.Y. Lin, Y. Zhu, Y. Shen, J. Zhang, X. Han, L. Zhang, Z. Xia, Adv. Energy Mater. (2019) 1902625.
[54] W. Zheng, J. Yang, H. Chen, Y. Hou, Q. Wang, M. Gu, F. He, Y. Xia, Z. Xia, Z. Li, B. Yang, L. Lei, C. Yuan, Q. He, M. Qiu, X. Feng, Adv. Funct. Mater. (2019) 1907658.
[55] L. Wang, W. Chen, D. Zhang, Y. Du, R. Amal, S. Qiao, J. Wu, Z. Yin, Chem. Soc. Rev. 48 (2019) 5310–5349.
[56] Z. Liang, W. Guo, R. Zhao, T. Qiu, H. Tabassum, R. Zou, Nano Energy 64 (2019) 103917.
[57] E. Gileadi, Wiley-VCH, Weinheim, Germany, 1993.
[58] M. Zhao, Y. Gu, P. Chen, Z. Xin, H. Zhu, B. Wang, K. Zhu, S. Yan, Z. Zou, J. Mater. Chem. 7 (2019) 9316–9323.
[59] M. Gattrell, N. Gupta, A. Co, J. Electroanal. Chem. 594 (2006) 1–19.

Dr. Yan Lu is currently an ARC DECRA Fellow at the University of Wollongong, Australia. She obtained her PhD degree from Shanghai Institute of Ceramics, Chinese Academy of Sciences in 2014, under the supervision of Prof. Zhaoyin Wen. From 2014 to 2018, she was a postdoctoral research fellow at Nanyang Technological University, Singapore. Her research focuses on the rational design and controllable fabrication of complex nanostructured functional materials and their applications for rechargeable batteries and efficient electrocatalysis.

Haojing Wang received her B.S. from Rutgers University in 2017. She is currently a Ph.D. candidate under the supervision of Professor Rong Xu at the School of Chemical & Biomedical Engineering, Nanyang Technological University (NTU). Her research interest focuses on the synthesis of nanomaterials for photocatalytic and electrocatalytic CO_2 reduction.

Dr. Pengfei Yu received his Ph.D. degree in Physical Chemistry at Shanghai Institute of Ceramics, Chinese Academy of Sciences in 2014. He is currently an assistant researcher at Shanghai Institute of Microsystem and Information Technology, Chinese Academy of Sciences. His main interest lies in getting deep insight into the intrinsic interactions in electrochemical energy materials from the point of local structure and electronic structure utilizing multiple synchrotron X-ray techniques and exploring their roles in electrochemical performances.

Dr. Yifei Yuan obtained his Ph.D. from Michigan Technological University and is currently holding a research assistant professor position at University of Illinois, jointly with Argonne National Laboratory. His research focuses on advanced electron microscopic and spectroscopic characterizations in functional nanomaterials for energy-related application.

Dr. Shahbazian-Yassar is currently a professor at the Department of Mechanical and Industrial Engineering at University of Illinois at Chicago. Prior to this position, he was an assistant and then associate professor at Michigan Technological University. He received his Ph.D. in Materials Science from Washington State University. His research focuses primarily on in-situ TEM studies of nanomaterials. He has published more than 200 peer-reviewed journal articles.

Dr. Yuan Sheng is a research fellow at the School of Chemical & Biomedical Engineering, Nanyang Technological University (NTU) and Cambridge Centre for Advanced Research and Education in Singapore (CARES). He obtained his Ph.D. degree at the National University of Singapore in 2016. His research interest includes gas-phase synthesis of nanomaterials, water splitting, and CO_2 utilization.

Shuyang Wu is currently a Ph.D. student under the supervision of Prof. Rong Xu at Nanyang Technological University, Singapore. He obtained his B.E. degree in School of Chemical Engineering at Dalian University of Technology (2014) and M.S. degree in Viterbi School of Engineering at University of Southern California (2016). His research focuses on the flame synthesis of nanostructured materials for energy and environmental applications.

Dr. Wenguang Tu is currently a research fellow in Nanyang Technological University (NTU), Singapore. He obtained his Ph. D. degree from School of Physics, National Laboratory of Solid State Microstructures, Nanjing University, China. His research interest includes the synthesis of nanomaterials for photocatalysis.

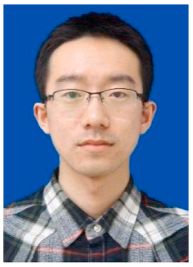

Dr. Guanyu Liu is a research fellow at the School of Chemical & Biomedical Engineering, Nanyang Technological University (NTU) and Cambridge Centre for Advanced Research and Education in Singapore (CARES). He received his Ph.D. degree at the Australian National University in 2017. His research is focused on the nanostructured catalysts for (photo)electrochemical water splitting and carbon dioxide reduction.

Prof. Markus Kraft is a Fellow at Churchill College and Professor in the Department of Chemical Engineering and Biotechnology at the University of Cambridge. He is Director of CARES Ltd, the Singapore-Cambridge CREATE Research Centre. He studied mathematics and received his doctorate in technical chemistry from the University of Kaiserslautern in 1997. After working for the University of Karlsruhe and the Weierstrass Institute for Applied Analysis and Stochastics in Berlin he became a lecturer at the University of Cambridge in 1999. He is a Fellow of the Combustion Institute and is an expert on the flame synthesis of nanoparticles.

Prof. Rong Xu is a Professor at the School of Chemical & Biomedical Engineering, Nanyang Technological University (NTU), Singapore. She received her Ph.D. degree at the National University of Singapore in 2004. Her research group has been actively involved in areas related to energy and environmental applications including solar fuel generation and water treatment, using nanoengineered particulate semiconductor photocatalysts, molecular complexes, and hybrid systems.